JOURNAL OF APPLIED POLYMER SCIENCE VOL. 11, PP. 963–981 (1967)

Delayed Yielding of Epoxy Resin Under Tension, Compression, and Flexure. I. Behavior Under Constant Strain Rate

ORI ISHAI, *Department of Mechanics, Technion, Israel Institute of Technology, Haifa, Israel*

Synopsis

Series of loading tests were carried out on epoxy resin specimens, at varying constant strain rates, under tension, compression, and flexure. The stress–strain relationship revealed a distinct yielding stage followed shortly by a post-yielding region of decreasing load. In all cases, results indicate linearity between yield stress and log strain rate, in accordance with Eyring's theory of viscous flow. For specimens unloaded close to the yield point, photoelastic observations revealed a residual pattern parallel to the theoretical principal shear stresses. These results, supported by additional data from other works, indicate a viscoplastic deviatoric stress-biased diffusional mechanism as the dominant factor in the yielding of an amorphous crosslinked epoxy system.

INTRODUCTION

Yielding is commonly related to the plasticity and ductile behavior of crystalline solids and attributed to activation and motion of dislocations within the crystal lattice. Yielding of glassy amorphous and semicrystalline polymers had not been widely investigated in the past, but is now drawing more attention on account of the technologically important mechanism of cold-drawing.

Reviews[1,2] and works[3,4] on this subject discuss yielding characteristics in general, as well as those of certain polymers under constant strain rate, mainly polystyrene,[5–7] nylon 66,[8–10] and polyethylene.[11–13]

Several hypotheses were suggested and discussed, but the micro- and macromechanisms involved are still obscure. The adiabatic theory, proposed by Marshall and Thompson,[14] attributes the drawing process to local heating of the material above its softening point. Experimental evidence and calculations rule out heat as the dominant factor.[3,9,15] A modified theory by Vincent[4] is based on reduction of Young's modulus through heating due to adiabatic stretching, with resulting higher curvature of the stress–strain relationship up to a level of instability reflected in yielding and necking.

Zaukelies[8] has proposed a crystal-defect model and a dislocation-motion mechanism for semicrystalline polymers. This was supported to some extent by observation of deformation bands oriented along the theoretical

shear field in tension and compression[16–18] analogous to the crystalline Lüder lines.

Objections to a general dislocation-model theory for polymers may be summed up as follows:

(*a*) Yielding and ductility are a common property of several amorphous polymers, for which the dislocation concept is somewhat meaningless.

(*b*) Permanent deformation during yielding and cold-drawing was found to be thermorecoverable.[3,17]

(*c*) Strong dependence of the yielding characteristics on time and temperature is evident, and qualitatively common to both amorphous and semicrystalline polymers.[3,5,19]

The above reasoning does, however, indicate that yielding in glassy polymers is mainly attributable to a viscous-flow mechanism activated at high shearing stress (or deviation-energy) levels, and governed by the activation energy and a stress-biased diffusional process. Such a mechanism for cold-drawing was suggested by Lazurkin[3] and Robertson.[19] Yielding in semicrystalline polymers was attributed by Hookway[20] to segmental motion within the amorphous regions. From the macrorheological point of view, yielding in glassy polymers could be related to viscoplasticity or termed "athermal inelasticity" (according to Freudenthal[21]). It could thus be represented by Eyring's theory of viscous flow[22] under high stresses and at low temperature levels.[19,23]

Under a constant strain rate this mechanism originates probably where deviation from linear viscoelastic behavior sets in below the apparent yield point. Closer examination of the stress–strain relationship is thus essential.

The typical tensile stress–strain curve under a constant strain rate may be divided, in principle, into five distinct regions (Fig. 1):

1. Under low stresses, up to the proportionality limit B, linearity is almost perfect, and both strain and strain energy are recoverable elasticity after unloading.

2. Above point B, deviation from linearity is accompanied by anelastic hysteresis—i.e. full deformational (delayed) recovery is expected, with energy dissipation reflected in the hysteresis loop; linear viscoelastic behavior is assumed up to a theoretical point C.

3. Above point C, deviation from linear viscoelasticity and long-term deformational irrecoverability indicate plastic behavior; this level could be defined here as the "onset of yielding." The rate of energy dissipation increases steeply above C, apparently until it has offset the rate of external energy supply by the loading machine at the yield point D.

4. The short plateau D–E may be described mathematically as $d\sigma = 0$, where $\sigma = f(\epsilon,t)$; it is defined here as the "yielding plateau."

5. Beyond point E, in the post-yielding region, a pronounced dimensional change is noticeable in the case of nonhomogeneous deformation; it is associated with marked local necking.

The plot may follow one of two distinct courses:

(I) E–F. In the case of the brittle–ductile behavior characterizing

rigid glassy polymers,[4,7] a monotonic stress decrease terminates shortly in a brittle fracture at a lower stress level (F). In this case point E may be defined here as the "onset of instability". The cracking process which sets in the post-yielding region E–F is, however, rather slow, because of the high rate of energy dissipation through plastic flow. This mode of behavior is frequently observed at low temperature levels and high strain rates.[17]

(II) E–F. In cases of predominantly ductile behavior characterizing the cold-drawing process, the nominal stress drop is stabilized at a long-term minimum (almost constant) stress level, followed by a moderate stress increase up to ductile failure, often above the first yield-point.

The general behavior of polymers may thus be classified in four distinct modes of stress–strain relationship (Fig. 1):

(*a*) Brittle behavior, where brittle failure sets in before yielding.

(*b*) Brittle-ductile behavior, where brittle failure follows shortly after yielding (A–F).

(*c*) Dutile behavior (A–F′), with two yielding levels.

(*d*) Homogeneous behavior (A–F″), without typical yielding characteristics.

As demonstrated by Hsiao and Sauer,[5] polymers (even those with high brittle tensile characteristics) are expected to behave according to mode A–F′ under compressive loading.

The course up to point E is common to all plastics with ductile characteristics. Beyond this point we are dealing with a complex situation involving pronounced changes in properties and dimensions with time, stress, and deformation. The present work centers on the problem of yielding and its characteristics up to point E.

Most experiments on yield and rupture are conducted under tensile loading. It is believed, however, that a more general picture is obtainable by studying both the tensile and compressive behavior, including the relationship between the above simple modes and flexure, which is a common feature of most engineering structures, as well as of the standard impact tests.

The ductile type of epoxy mix used in the present work represents a relatively new family of thermosetting crosslinked polymers. In contrast to the extensive experimental work on the mechanical behavior of linear thermoplastic polymers, only few studies have dealt with epoxy systems. Recent papers on this subject[24–26] conclude that in the vicinity of their glass temperature and above it, epoxy resins exhibit characteristics similar to those of other amorphous polymers as regards linear viscoelasticity, the time–temperature superposition principle, and ultimate tensile behavior. The versatility of epoxy resins, covering a wide range of properties from strong and brittle to ductile and tough, is an important experimental advantage. Its capacity for stress-induced birefringence[24,27,28] provides a valuable qualitative tool for orientation studies. The present paper reports part of the experimental findings of an extensive study. The

second part, to be published shortly, will deal with behavior under constant stress (creep), and include a theoretical analysis of both parts.

EXPERIMENTAL PROCEDURE

Preparation of Specimens

A cold-setting mix of Versamide 140* and Shell Epicote 815 was used. Preliminary tests on cured resins, consisting of 30/70 and 40/60 Versamide–Epicote, respectively, resulted in brittle failure with no apparent yielding at high strain rates. A 50/50 mix was found suitable for the present work, because of the high ductility of the hardened product.

The liquid mixture was cast in rectangular Teflon molds, 20/20/400 mm. (which saved the use of release agents) and cured at room temperature (23–25°C.) for 48 hr. After demolding the specimens were transferred to a climate room (23°C. ±1, 70–80 R.H.) for additional setting for 12 days. At 14 days three types of specimens were prepared according to the three modes of loading used, namely 7-mm. thickness, 12-mm. width, and 120-mm. gage length for tension (Fig. 2*a*), cyclindrical–18 mm. diameter and 36 mm. height–for compression (Fig. 2*b*), and rectangular—20/16/190 and 20/16/130—for flexure (Fig. 2*c*). Machining was carried out with extreme care, to avoid residual stresses.

Test Procedure

Tests were conducted at almost constant temperature, 26 ± 1°C. Fluctuations of 1–2°C. had an insignificant effect on the yielding characteristics investigated.

Specimens were mounted on an Instron tester and loaded at a constant rate of displacement (crosshead speed) ranging from 0.1 to 50 mm./min.† Centricity of the load in the tensile specimens was checked by photoelastic means. The contact surfaces of the cylinders were coated with molybdenum disulphide paste to reduce lateral friction in compression. The actual state of stress under this mode of loading was rather complicated, but results indicate good agreement with the tensile and flexural modes of behavior.

A special device was provided for the flexure tests. Specimens were mounted on rollers spaced according to the two spans tested, namely 8 and 16 cm. Central point-loading was applied through a smooth roller. A constant rate of central deflection was maintained, and the central load vs. central deflection (and time) was recorded.

* Versamide 140 serves both as curing agent and plasticizer. An increase in its content improves toughness, but probably reduces the crosslink density of the final product.

† Preliminary measurements, using optical and electrical strain gage techniques, revealed near-linearity between local strains and the total displacement recorded by the Instron. It is thus safe to assume that a constant strain rate was maintained during loading.

Six series of tests were run as follows:

Series a. Loading Up to Ultimate Value. For qualitative purposes, a single specimen was loaded at each speed-making a total of 8 × 4 for the four types of specimens and three modes of loading. In the tension and flexure tests, the series terminated in fracture. In the case of compression, where no fracture occurred, loading was discontinued when marked eccentricity developed due to progressive distortion of the specimen.

Series b. Loading Up to Yield. This series comprised at least 2 × 8 specimens for each mode, loaded up to yield and unloaded approximately at the onset of load decrease. Most of these specimens were used again later in series d.

Series c. Repeated Cycles of Loading Up to Yield and Unloading. This series comprised tensile specimens loaded up to yield and reloaded on reversal of the slope, using the Instron slope detector. Immediately at zero load, the specimens were reloaded at the same speed following the same course, and the cycles repeated up to fracture.

Series d. Influence of Loading and Curing History. This series, in which most of the specimens of series b were used, dealt with the reproducibility of the general trend observed in the first cycle, and with the influence of previous yielding on subsequent stress–strain relationships. Heat treatment was applied for annealing residual stresses. The sequence was as follows, with at least one-day intervals between successive loadings: Cycle I, first loading up to yield; Cycle II, second loading up to yield: (creep tests under high stresses); Cycle III, loading up to yield; Cycle IV, loading up to yield; Cycle V, loading up to yield following heat treatment at 80°C. for 2 hr. (creep tests under high stresses); Cycle VI, loading up to yield following heat treatment, as before.

Series e. Photoelastic Examination. This auxiliary technique was confined to qualitative detection of residual effects due to yielding. Virgin specimens were loaded in tension up to a given extension (or stress) level, unloaded, reloaded after a short interval up to a higher level at the same

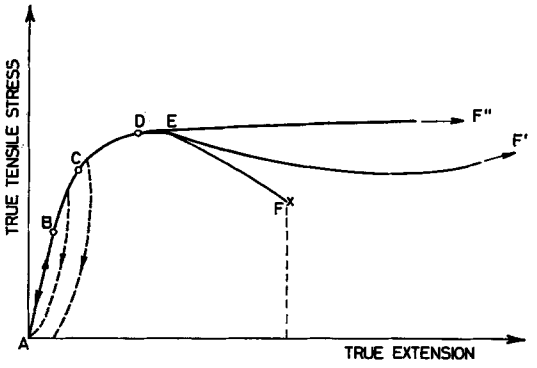

Fig. 1. Typical stress–strain relationship representing different modes of ductile behavior of polymers.

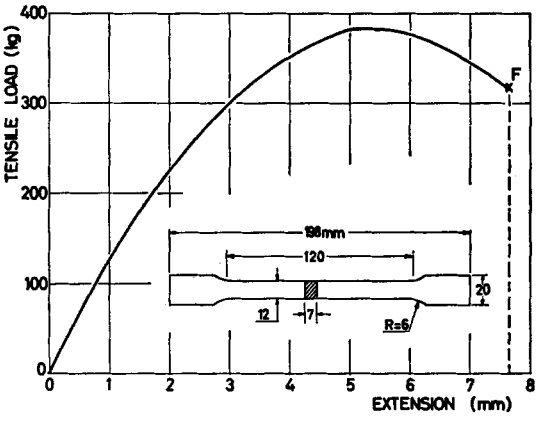

(*a*)

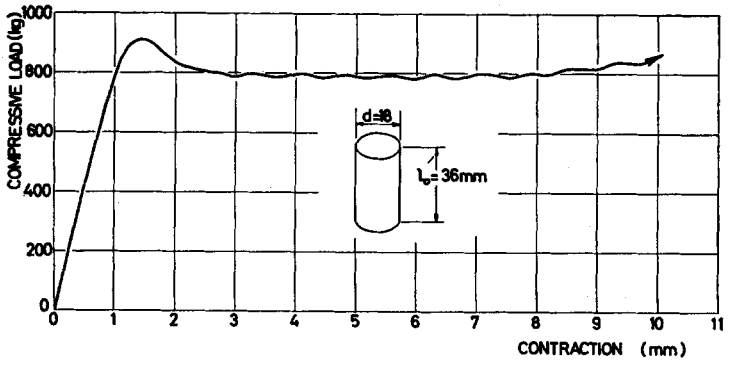

(*b*)

Fig. 2. See caption, p. 969.

rate, unloaded again, and so on up to the yield region. Each specimen was placed between two circular polaroids and examined in artificial light, before and during loading, immediately after unloading, 24 hr. after the test (at room temperature), and finally after heat treatment.

Series f. Central Deflections vs. Longitudinal Strain in Flexure. This series, carried out at three crosshead speeds, provided quantitative data for expressing the constant central deflection rate in longitudinal terms. Electrical strain gages were glued at the upper and lower extremes of the specimen midsection and used for compressive and tensile strains readings simultaneously with those of central deflection.

The series was limited to the low stress range by the capacity of the strain gage used (up to about 8000 microstrains).

RESULTS AND DISCUSSION

Series a

Load vs. deformation curves indicate a common trend up to point E of Figure 1; a linear region, a curved region and a short "yield plateau," especially pronounced under tensile loading (Fig. 2*a*).

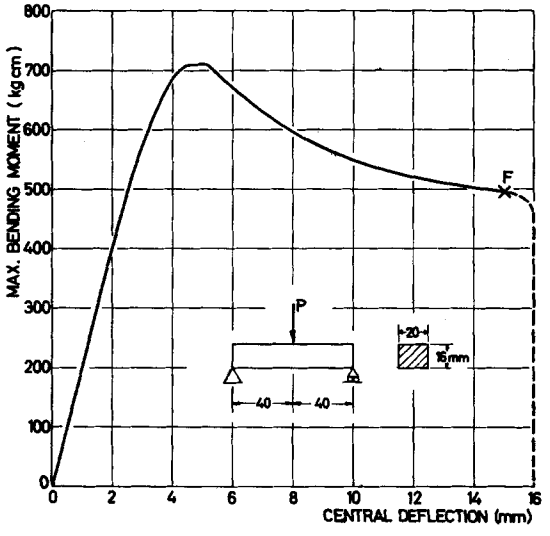

(c)

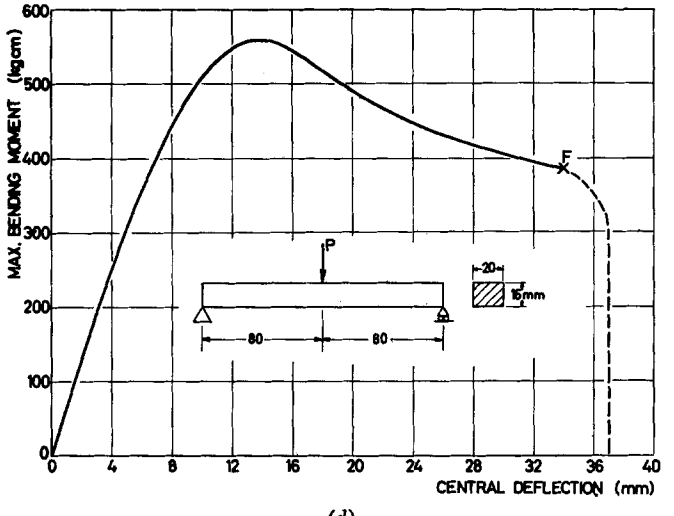

(d)

Fig. 2. Typical load–deformation curves up to ultimate stage, for three modes of loading: (*a*) tension; (*b*) compression; (*c*) flexure.

Dissimilarity between the three modes of loading was apparent during the post-yielding stage:

In the tension tests, a monotonic load decrease, terminating shortly in brittle fracture, was accompanied by development of one to three local neckings. A crack, orginating at one of these, propagated slowly perpendicular to the tensile stress field (Fig. 3*a*).

A similar trend was observed in the flexure tests (Fig. 2*c*), with a moderate load decrease and a longer delay between yield and fracture. The crack

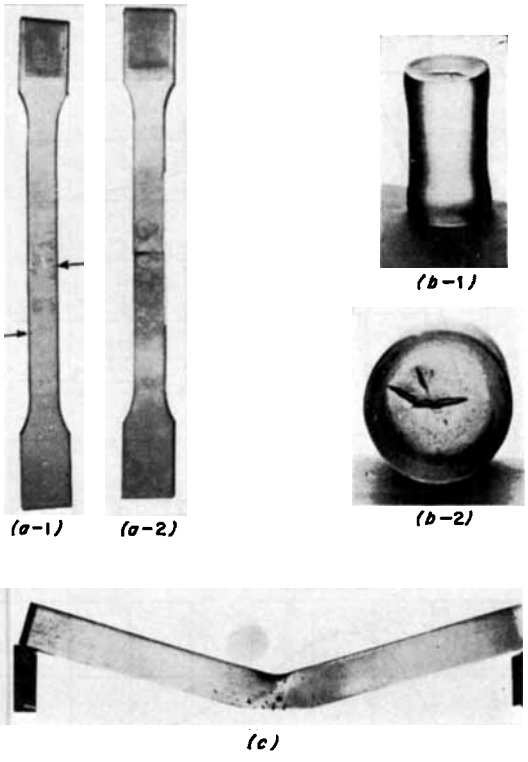

Fig. 3. Epoxy specimens loaded up to ultimate stage: (*a*-1) tension, (*a*-2) cracked, fractured; (*b*) compression, (*b*-1) front view, (*b*-2) upper view; (*c*) flexure.

in this case originated centrally at the tensile fibers and propagated upwards (Fig. 3*c*), accompanied by a considerable permanent deflection and pronounced lateral contraction on the tension side and extension on the compression side.

In the compression tests, a prolonged lower wave-like yield plateau was established (Fig. 2*b*). A moderate load increase was observed with marked lateral distortion mainly at the lower and upper faces. In extreme cases a crack developed parallel to the compressive stress field (Fig. 3*b*).

While only small recoverable dimensional changes were detected during the pre-yielding stage, the post-yielding stage was accompanied by considerable permanent distortion.

Series b

Families of stress–strain curves, up to yield, obtained in tension (Fig. 4) and compression (Fig. 5), exhibit the same common characteristics: A linear region followed by a curved region (terminating in a flat maximum at yield), both increasing with strain rate. The point of slope reversal at the end of the short "yield plateau" was chosen as criterion of the yield-de-

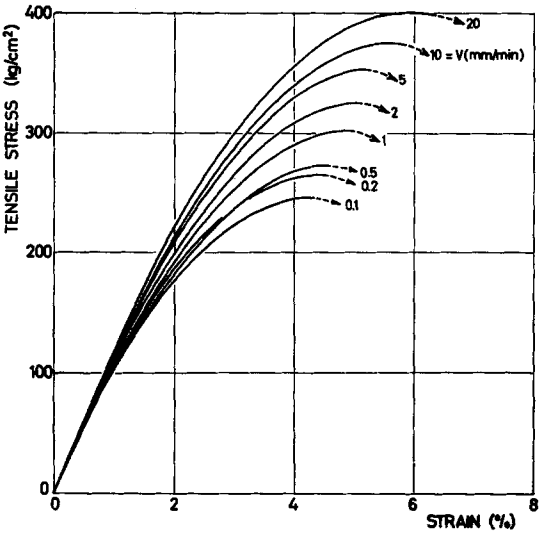

Fig. 4. Family of tensile stress–strain curves up to yield under different strain rates.

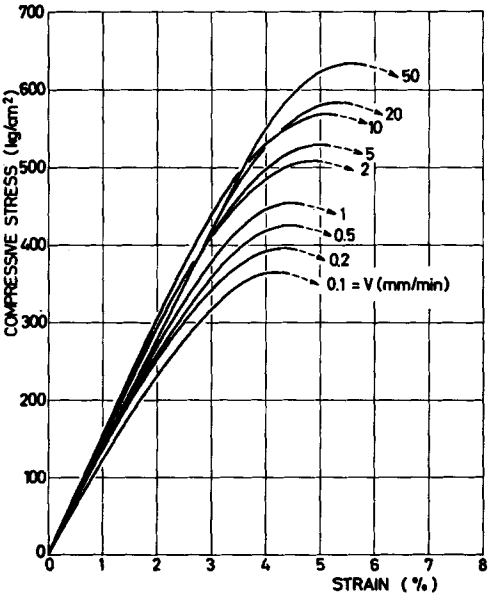

Fig. 5. Family of compressive stress–strain curves up to yield under different strain rates.

formation (δ_Y), -strain (ϵ_Y), and -time (t_Y). Almost no dimensional changes were detected in specimens unloaded at this stage, so that nominal stress and strain values could be regarded approximately as the true ones.

The same characteristics were found in the flexure tests (Fig. 6).

In all cases, similar trends were obtained for 2–3 equivalent groups for each mode of loading, which justifies the use of one group as representative.

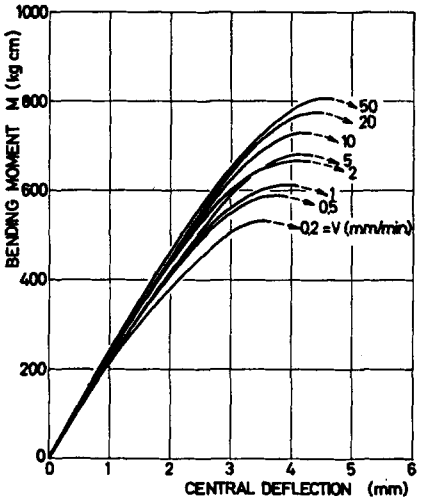

Fig. 6. Family of flexural moment–deflection curves up to yield under different deflection rates (beam span: $l = 8$ cm.).

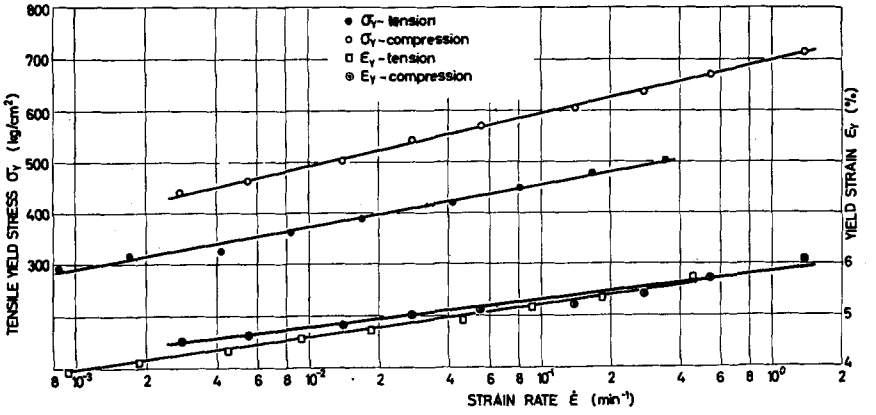

Fig. 7. Tensile and compressive yield stress and respective yield strains vs. log strain rate.

Linearity was found between the tensile and compressive yield stress and strain and the log strain rate (Fig. 7). The same applies to yield stress vs. log yield time (Fig. 8). The compressive yield level is 20–30 higher than its tensile counterpart. Dependence of the yield strain on strain rate is less pronounced, but apparently the same for both tension and compression. Similar linearity was established between the yield moment on the one hand and log deflection rate and yield time on the other (Figs. 9, 10).

Young's modulus in tension and compression was obtained from the initial slopes of the stress–strain curves (Figs. 4, 5). In both cases it shows a similar moderate increase with strain rate (Fig. 11), with higher values for the compressive modulus.

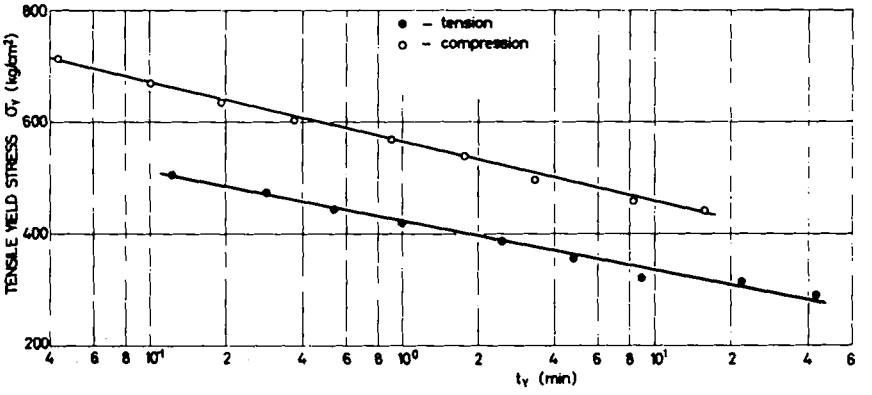

Fig. 8. Tensile and compressive yield stress vs. log yield time.

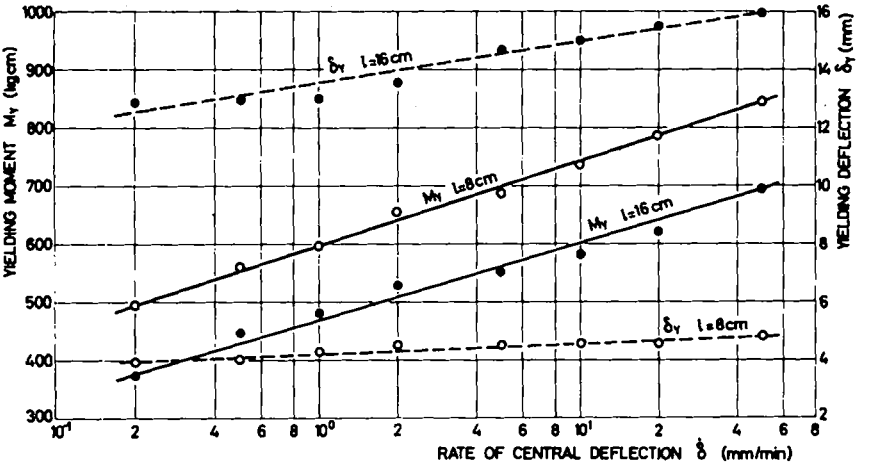

Fig. 9. Yield moment and yield deflection vs. log deflection rate (flexure).

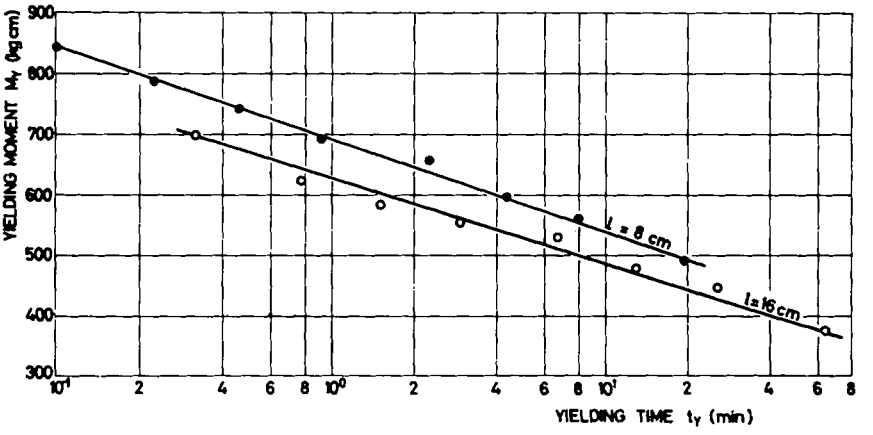

Fig. 10. Yield moment vs. log yield time (flexure).

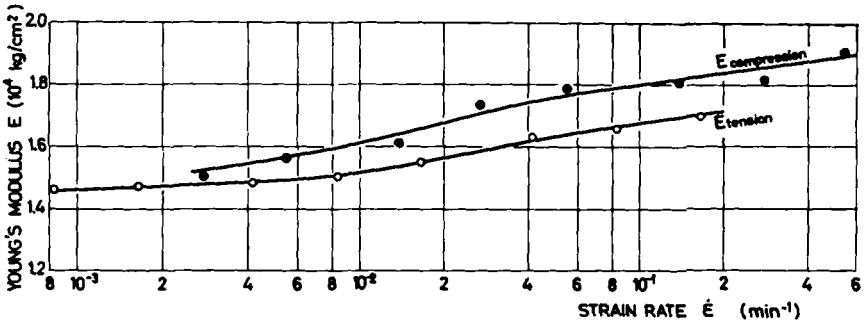

Fig. 11. Tensile and compressive Young's modulus vs. log strain rate.

Series c

The following qualitative characteristics were obtained (Fig. 12): the yield stress at second loading was about 20% lower compared with the first. Subsequent cycles showed a small drop in the yield level, tending to a constant minimum maintained for 3–4 cycles. The final cycle, however, resulted in brittle failure at a still lower level.

The "yield plateau" lengthened from cycle to cycle, with a pronounced horizontal region. By contrast, the linear region became smaller (lower proportionality limit), and apparently disappeared at about the fourth cycle. (In other words, the stress–strain curvature increased). However, the tangent modulus at the origin remained almost unchanged throughout all cycles except the last, characterized by a lower initial slope. As marked necking was detected in the preceding cycle, the drop in the tangent modulus in the final cycle is attributable to the "onset of instability."

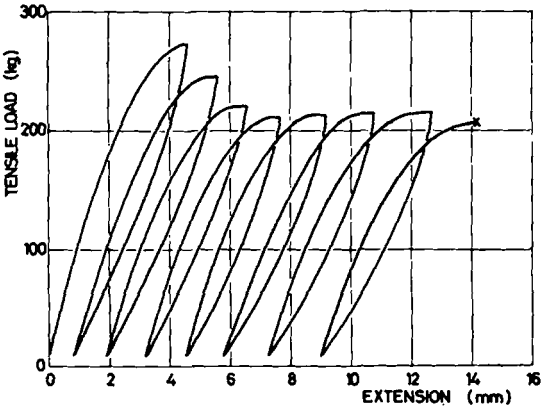

Fig. 12. Typical load–extension curves for repeated tensile loading and unloading cycles.

Series d

Loading history and heat treatment showed almost no effect on the stress–strain rate relationship in tension (Fig. 13), as indicated by the ap-

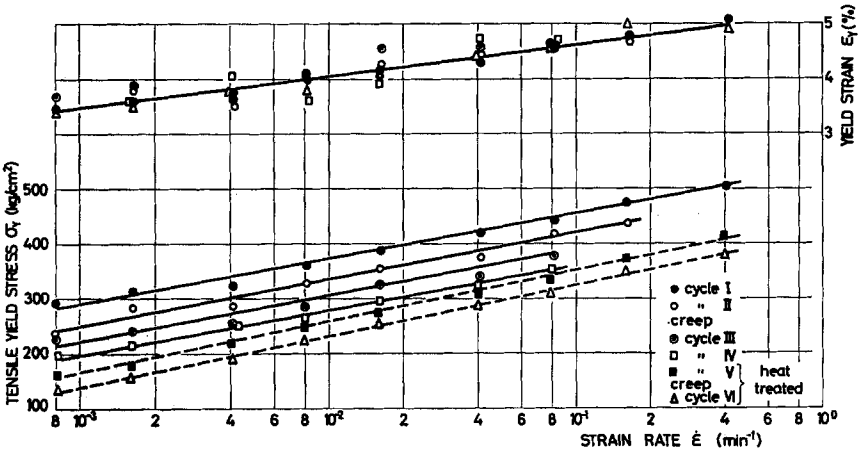

Fig. 13. Influence of loading and curing history on tensile yield stress and yield strain levels at different strain rates.

proximately same constant slope of the curve throughout all cycles. It did, however, clearly affect the yield stress level, as reflected in its gradual decrease from cycle to cycle. The yield strain seems to be entirely unaffected by the loading history, but high scatter is evident following the first cycle, probably due to residual stresses and strains accumulated during preceding cycles. This is, however, remedied by heat treatment, probably through diffusional recovery. Heat treatment seems also to increase stress–log strain rate slope.

Similar characteristics were observed in the compression and flexure tests.

Series e

Photoelastic examination revealed two important features:

On unloading during the linear region, all birefringence properties were restored, and subsequent loading resulted in the same color sequence as before. By contrast, on unloading beyond the linear region, below the yielding point, the pattern was quite different (Fig. 14*b*) and comprised bands of colored lines (at about 45° to the tensile axes*), which became denser as the yield level was approached. On unloading after slope reversal at least one dead zone was observed (Figs. 14*c*, 15*c*, 16*b*,*c*) and subsequent loading revealed loss of stress-induced birefringence sensitivity (S.B.S.) in these zones. Reloading of specimens previously subjected to considerable plastic deformation also revealed almost total loss of S.B.S. in all three modes.

Most of the residual patterns formed during loading disappeared on prolonged storage at room temperature, but in the vicinity of the necking regions the pattern was apparently permanently preserved under isothermal conditions (Figs. 14*d*, 16*c*). For all loading histories and modes heat-

* Coincident with the theoretical direction of maximum shear stress in pure tension.

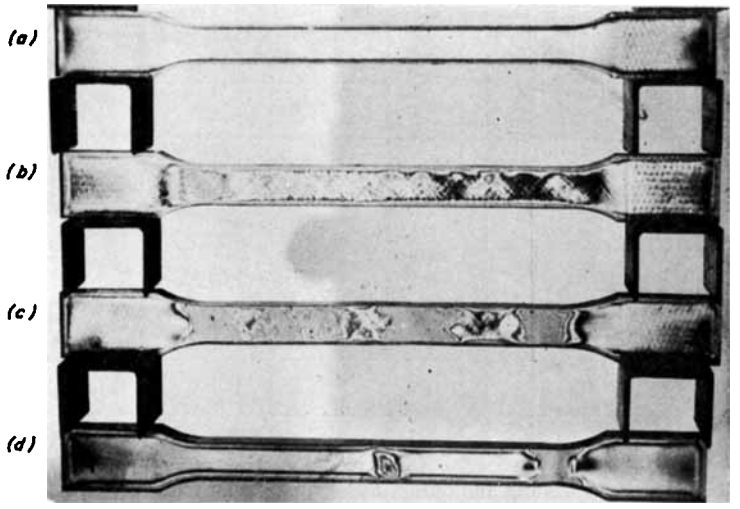

Fig. 14. Photoelastic pattern in tension: (*a*) virgin specimen before first loading, (or specimen heat-treated after yielding); (*b*) specimen unloaded shortly below yield (C–D regions); (*c*) specimen unloaded in post-yielding stage; (*d*) specimen unloaded in post-yielding stage and stored for a few weeks at room temperature. (Circular polaroids and transmitted daylight were used.)

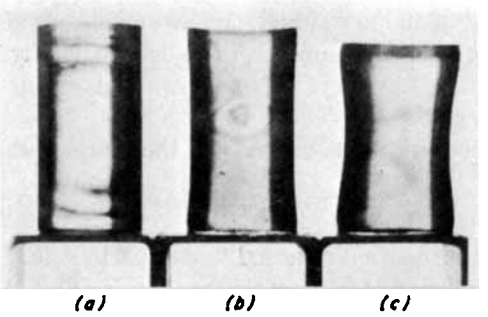

Fig. 15. Photoelastic pattern in compression: (*a*) virgin specimen before first loading, or specimen heat-treated after yielding; (*b*) specimen unloaded shortly beyond yield (note residual pattern at the center); (*c*) specimen unloaded in post-yield stage (residual pattern disappears). (Circular polaroids and transmitted daylight were used.)

treated specimens, except the cracked ones, recovered almost to their original state by regaining both their normal S.B.S. and initial dimensions.

Series f

Linearity between central deflection (δ) and maximum longitudinal strain (ϵ) was evident at low stress levels. The ratio $k = \epsilon/\delta$, however, seems to deviate considerably from that predicted by the elastic theory for pure flexure* (see Table I).

* See Appendix.

Compressive flexural strains are slightly smaller than the tensile ones. The strain rate seems to have almost no influence on k.

The discrepancy between theoretical and experimental values is attributable to several causes, such as unjustified disregard of the shear strains and other approximations involved in the elementary theory of

TABLE I
Theoretical and Experimental Values of k

Beam span l, cm.	k_{theor}, cm.$^{-1}$	k_{exp}, cm.$^{-1}$
8.0	15×10^{-2}	8.2×10^{-2}
16.0	3.75×10^{-2}	3×10^{-2}

elasticity for rigid solids, which are inapplicable to glassy polymers; another cause could be the high h/l ratio in the present case.

However, considering the linearity between σ_Y and log $\dot{\epsilon}$, variation of $\dot{\epsilon}$ by a factor of 2 or less would not affect the general trend.

Conversion of $\dot{\delta}$ into $\dot{\epsilon}$ was based on experimental k values, and derivation of the flexural yield stress σ_Y on calculation given in the Appendix.

As a result, the flexural data of Figures 9 and 10 may now be interpreted in terms of longitudinal stresses and strains as plotted in Figure 17.

Comparison with the corresponding relationship obtained from pure tension and compression tests (reproduced from Figs. 7 and 8 in solid lines)

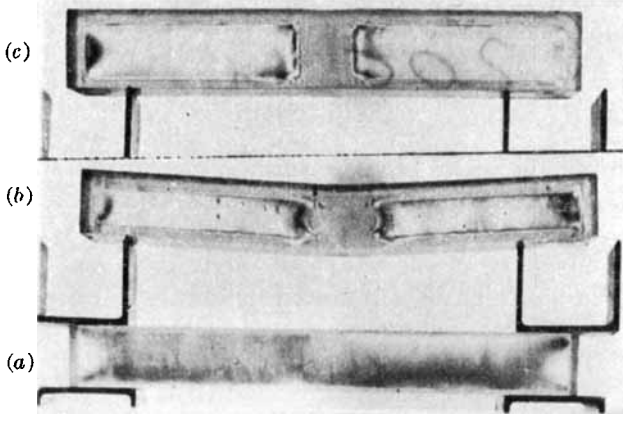

Fig. 16. Photoelastic pattern in flexure: (*a*) virgin specimen before first loading or specimen heat treated after yielding; (*b*) specimen unloaded beyond yield (front view); (*c*) specimen unloaded beyond yield (bottom view). (Circular polaroids and transmitted daylight were used.)

shows good agreement for the longer beam and higher values for the shorter one. In both cases, however, almost the same slope as before is obtained for σ_Y versus log $\dot{\epsilon}$. The higher level for the shorter beam is attributable

also to interaction of shear stresses and lateral constraints. Good correlation of the behavior under the three modes of loading, which involve

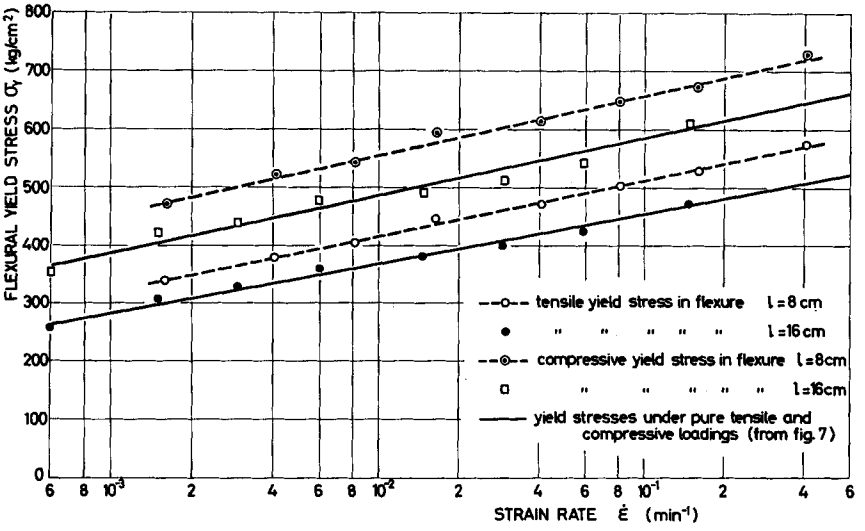

Fig. 17. Tensile and compressive yield stresses in flexure vs. longitudinal beam strain rate (from Fig. 9), compared with the same relationships under pure tensile and compressive loading (from Fig. 7, in solid lines).

four variants of geometry, is evident by the relations of log yield time vs. log strain rate demonstrated in Figure 18.

CONCLUSION

Loading of ductile epoxy resin specimens under a constant strain rate reveals a clear yielding stage followed by stress decrease. Linearity between yield stress and log strain rate (or log yield time) was established for tensile, compressive and flexural modes of loading.

This relationship could be formulated for the isothermal glassy state, according Eyring's theory of viscous flow at high stress and low temperature levels. The above evidence is also in agreement with photoelastic observations of the residual shear pattern, as well as with the fact of almost full dimensional recovery after heat treatment. It is thus justified to assume a viscoplastic mechanism as the one prevailing in the present case, which also represents other amorphous polymer systems in the glassy state under high stress.

Yielding of such materials is another form of a viscous flow which becomes fully activated only beyond a certain level and under a certain rate of external mechanical energy supplied by the loading apparatus. Such a

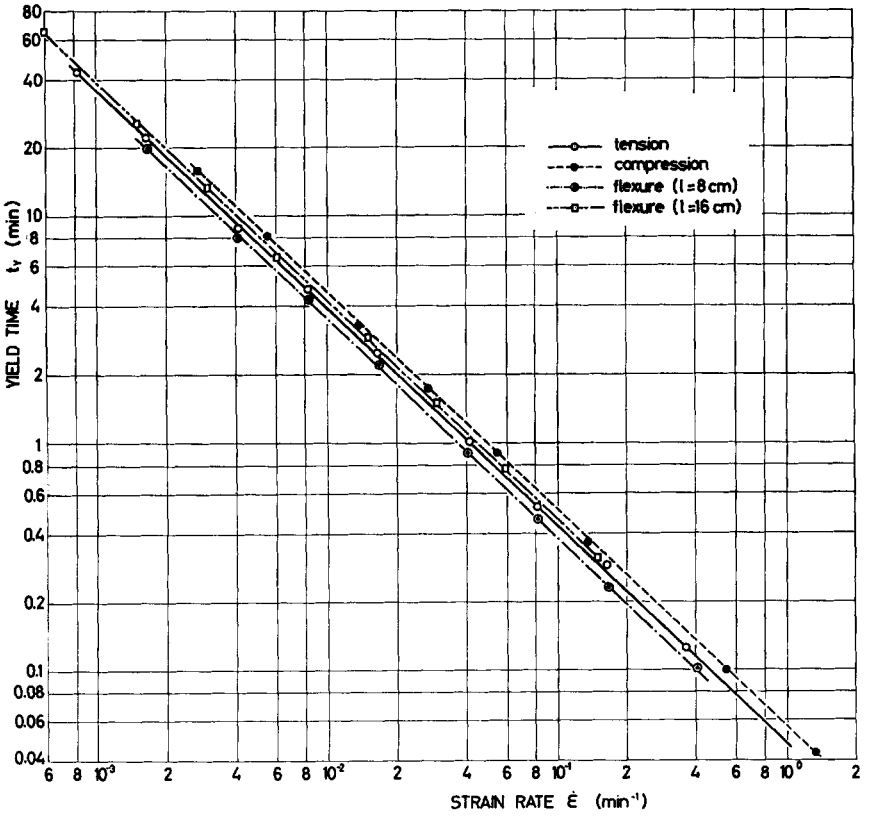

Fig. 18. Yield time vs. longitudinal strain rate under tensile, compressive, and flexural modes of loading.

mechanism is governed by deviatoric energy and oriented by the principal shear stresses. The yield level is thus, expected to be closely dependent on time or strain rate.

Four principal regions were distinguished by analyzing the stress–strain relationship:

(*a*) A linear anelastic region under lowstress, during which the material probably behaves according to linear viscoelastic laws.

(*b*) Deviation from viscoelastic linearity, indicating the onset of internal destruction processes.

(*c*) A yielding region, where temporary equilibrium is established between the rates of external energy supply and energy dissipation through microdestruction (scission) of secondary bonds.

(*d*) Onset of instability indicated by the decrease in stress level, where microfailure probably develops into macrocracks which propagate slowly in a brittle–ductile manner, up to the final stage of fracture.

APPENDIX

Interpretation of Flexural Data

Yield stresses in flexure are obtainable assuming flexural yield to occur when the entire midsection of the beam is in plastic flow and behaving like a plastic hinge. This assumption is borne out by photoelastic evidence—loss of S.B.S. over the entire midsection of the yielding beam (Figs. 16*b*, 16*c*).

The ratio of compressive-to-tensile yield stress (λ), obtainable from Figure 7, ranges from about 1.27 to 1.38 according to strain rate.

The relation between maximum yield moment and that of compressive and tensile stresses in flexure is obtainable on the approximate assumption of a rectangular stress diagram for the plastic zone of the beam, whereby:

$$\sigma_{Yt} = [2(1 + \lambda)/\lambda]\ (M_Y/bh^2) \tag{1}$$

where M_Y = yield moment (at midsection), σ_{Yt} = yield stress at the extreme tensile fibers, σ_{YC} = yield stress at the extreme compressive fibers $\sigma_{YC}/\sigma_{Yt} = \lambda$ = compressive-to-tensile yield stress ratio, and b,h = width and depth of beam cross-section, respectively.

Conversion of the deflection rate into longitudinal compressive or tensile strain rate at the extreme fibers of the beam is easily derived using the simple beam theory with shear strain neglected,

$$k = \epsilon/\delta = \dot{\epsilon}/\dot{\delta} = 6h/l^2 \tag{2}$$

where ϵ,δ, and $\dot{\epsilon},\dot{\delta}$ are the longitudinal strain, central deflection, and their time derivatives, respectively, l and h are the beam span and depth, respectively.

The author wishes to express his gratitude to E. Goldberg for editorial assistance and advice. He would also like to thank P. Shechter of the Department of Mechanics for help in conducting the tests and for the drawings.

References

1. L. E. Nielsen, *Mechanical Properties of Polymers*, Reinhold, New York, 1962, pp. 105–113.
2. P. D. Richie, *Physics of Plastics*, Plastic Institute, London, Iliffe, 1965, pp. 77–85.
3. J. S. Lazurkin, *J. Polymer Sci.*, **30**, 595 (1958).
4. P. I. Vincent, *Polymer*, **1**, 7 (1960).
5. C. C. Hsiao and J. A. Sauer, *ASTM Bull.*, **172**, 29, (1951).
6. R. G. Cheatham and A. G. H. Dietz, *Trans. ASME*, **74**, 31 (1952).
7. S. D. Eagleton, *Plastic Inst. (London) Trans. J.*, **24**, 250 (1956).
8. D. A. Zaukelies, *J. Appl. Phys.* **33**, 2797 (1962).
9. M. F. Bender and M. L. Williams, *J. Appl. Phys.*, **34**, 3329 (1963).
10. M. L. Williams and M. F. Bender, *Textile Res. J.*, **33**, 1023 (1963).
11. S. Newman, *J. Polymer Sci*, **27**, 563 (1958).
12. S. Newman, *J. Appl. Polymer Sci.*, **2**, 252 (1959).
13. S. Strella and S. Newman, *Polymer*, **5**, 107, (1964).
14. I. Marshall and A. B. Thomson, *Proc. Roy. Soc. (London)*, **221A**, 541 (1954).
15. R. G. Quynn, *J. Appl. Polymer Sci.*, **4**, 253 (1960).

16. W. Whitney, *J. Appl. Phys.*, **34**, 3633 (1963).
17. C. J. Speerschneider and C. H. Li, *J. Appl. Phys.*, **34**, 3004 (1963).
18. D. H. Ender and R. D. Andrews, *J. Appl. Phys.*, **36**, 3057 (1965).
19. R. E. Robertson, *J. Appl. Polymer Sci.*, **7**, 443 (1963).
20. D. C. Hookway, *J. Textile Inst. Proc.*, **49**, 292 (1958).
21. A. M. Freudenthal, *The Inelastic Behavior of Engineering Materials and Structures*, Wiley, New York, 1950, p. 137.
22. H. Eyring, *J. Chem. Phys.*, **4**, 283 (1936).
23. C. B. Arends, *J. Appl. Polymer Sci.*, **10**, 1099 (1966).
24. P. S. Theocaris, *Rheol. Acta*, **2**, 92 (1962).
25. P. S. Theocaris, *J. Appl. Polymer Sci.*, **8**, 399 (1964).
26. D. H. Kaelble, *J. Appl. Polymer Sci.*, **9**, 1213 (1965).
27. E. H. Dill and C. Fowlkes, *Trend Eng.*, **16**, 5 (1964).
28. P. S. Theocaris, *Exptl. Mech.*, **5**, 105 (1965).

Résumé

Des séries de tests de charge ont été effectués avec des échantillons de résine époxy à différentes vitesses de tension constante sous tension, compression et flexion. Les rapports tension–traction ont révélé des points de rendement distincts suivis rapidement par une région de post-rendement de la charge décroissante. Dans tous les cas, les résultats indiquent une linéairité entre la tension de rendement et le log de la vitesse de tension en accord avec la théorie de Eyring pour l'écoulement visqueux. Pour les échantillons non chargés au voisinage de leur point de rendement des observations photoélastiques ont révélés un réseau résiduel parallèle aux tensions de cisaillement principal théoriques. Ces résultats confirmés par des résultats ultérieurs d'autre travaux indiquent un mécanisme diffusionnel viscoplastique comme facteur dominant dans le rendement du systèmes époxy ponté amorphe.

Zusammenfassung

Belastungs-Testreihen wurden an Epoxyharzproben bei Variierung der konstanten Verformungsgeschwindigkeit unter Zug, Kompression und Verbiegung ausgeführt. Die Spannungs–Dehnungsbeziehung zeigte eine deutliche Fliessphase mit kurz darauf folgendem Nachfliess-Bereich bei abnehmender Belastung. In allen Fällen ergibt sich in Übereinstimmung mit der Theorie des viskosen Fliessens von Eyring eine lineare Beziehung zwischen Fliessgrenze und log Verformungsgeschwindigkeit. Bei Entlastung der Proben in der Nähe der Fliessgrenze zeigten Photoelastizitätsbeobachtungen zu den theoretischen Hauptschubspannungen parallele residuelle Figuren. Die Ergebnisse lassen, zusammen mit zusätzlichen Daten anderer Arbeiten, einen viskoplastischen, deviatorischen, spannungsbeeinflussten Diffusionsmechanismus als beherrschenden Faktor beim Fleissen eines amorphen vernetzten Epoxysystems erkennen.

Received November 30, 1966
Prod. No. 1537